Construction and Building Materials 262 (2020) 120001

Contents lists available at ScienceDirect

Construction and Building Materials

journal homepage: www.elsevier.com/locate/conbuildmat

Out-of-plane (flatwise) behavior of through-tenon connections using the integral mechanical attachment technique

Aryan Rezaei Rad [a,c,*], Henry Burton [b], Yves Weinand [a,c]

[a] Laboratory for Timber Construction (IBOIS), École Polytechnique Fédérale de Lausanne (EPFL), 1015 Lausanne, Vaud, Switzerland
[b] Department of Civil and Environmental Engineering, University of California Los Angeles (UCLA), 90095 Los Angeles, CA, USA
[c] The National Centre of Competence in Research (NCCR) Digital Fabrication, 8093 Zurich, Switzerland

HIGHLIGHTS

- Flatwise behavior of Integral Mechanical Attachments is experimentally studied.
- Small differences are observed between the yield and peak strengths.
- A brittle failure is observed in fiber- perpendicular specimens.
- The joints are mainly classified as having low ductility.

ARTICLE INFO

Article history:
Received 15 January 2020
Received in revised form 16 June 2020
Accepted 17 June 2020

Keywords:
Integral mechanical attachment technique
flatwise behavior
out-of-plane force–deformation behavior
through-tenon joints
timber plate structures
digital fabrication
physical experiments

ABSTRACT

This paper aims to characterize the force–deformation response of through-tenon wood-wood connections subjected to out-of-plane (flatwise) loads. Six beech LVL timber specimen groups with variations in the fiber orientation (parallel and perpendicular) and tab insertion angle (45°, 60°, and 90°) are tested. Minimal replicate-to-replicate variability for each specimen group was observed. Overall, the specimens reached their maximum capacity soon after yielding. Furthermore, the joints are classified as having low ductility. For the specimens where the main fibers are oriented perpendicular to the loading direction, low strength and brittle failure were observed. The yield and maximum strengths and the slip modulus were not affected by the tab insertion angle and therefore remained almost constant among these specimens. For the specimens where the main fibers are oriented parallel to the loading direction, higher strength and more ductile behavior was observed. The following mechanisms contributed to the load-deformation response of these specimens: inter-fiber layer resistance, tension–compression, flexural, shear and torsional resistance of the fibers, and the embedment compression resistance. Furthermore, the damage propagation was not concentrated in a specific location/surface. The notch size was found to have a strong influence on the yield and maximum strengths, as well as the slip modulus of the 45°-angled specimens.

1. Introduction

1.1. Integral mechanical attachment (IMA) technique in spatial timber plate structures

Wood-Wood connections - also referred to as integral mechanical attachments (IMAs) or carpentry joints - are the oldest known method of timber joinery [1]. The defining feature of IMAs is that the connection between timber elements is established solely through geometric manipulation, without additional connectors such as nails, screws, dowels, adhesives, and welding [2,3]. The through-tenon (TT) joint (Fig. 1a) is one common type of IMA [2]. The introduction of engineered timber products such as Laminated Veneer Lumber (LVL) boards, advancements in digital geometry processing using Computer Aided Design (CAD), and robotic/digital fabrication using Computer Numerical Control (CNC) machines, have revitalized the application of TT joints in structural engineering practice [3].

The performance of TT joints under different load conditions has been widely investigated. Using beech LVL (see [4] for more information) as the construction material, the tensile load-

* Corresponding author at: Laboratory for Timber Construction (IBOIS), École Polytechnique Fédérale de Lausanne (EPFL), 1015 Lausanne, Vaud, Switzerland.
E-mail addresses: Aryan.Rezaeirad@epfl.ch (A. Rezaei Rad), hvburton@seas.ucla.edu (H. Burton), yves.weinand@epfl.ch (Y. Weinand).

https://doi.org/10.1016/j.conbuildmat.2020.120001
0950-0618/

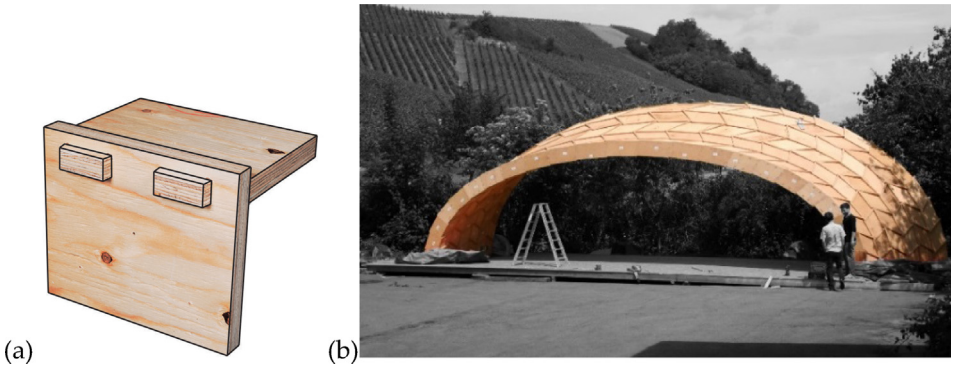

Fig. 1. (a) Through-tenon (TT) wood-wood connections, (b) prototype of an integrally-attached timber plate structure (photo credit: the laboratory for timber construction, IBOIS, at École Polytechnique Fédérale de Lausanne (EPFL) (https://www.epfl.ch/labs/ibois/) (the prototype was constructed by ANNEN SA, http://www.annen.eu/).

carrying capacity of TT joints was experimentally investigated by Rezaei Rad et al. [2]. In a separate study, the same authors examined the in-plane (edgewise) push-out force–deformation behavior of TT joints [3]. They concluded that (i) the timber fiber orientation plays an important role in the overall response, (ii) the TT joints are dominated by brittle failure mechanisms, and (iii) the tab insertion angle can significantly change the joint stiffness. Physical experiments were used by Roche et al. [5] to investigate the flexural response of TT joints. It was determined that IMAs can be designed to meet the requirements put forth in the European timber standard, Eurocode 5 [6]. Accordingly, Roche [7] concluded that IMAs can be potentially considered as an alternative to more conventional joinery methods (e.g. screw connections) in timber construction.

Recently, information-tool technology (see [8] for the definition) has given rise to the application of IMAs in timber plate structures through the use of 5-axis CNC robots. Using engineered planar boards, Robeller et al. [9], Magna et al. [10], Li and Knippers [11], and Krieg et al. [12] introduced an interlocking assembly for timber plates with IMAs positioned along their edges. The so-called edgewise connection was introduced, whereby multiple tabs are provided along the edge of a plate with the corresponding slots along its mate (Fig. 1a). This process of assembly enables full interlocking between neighboring structural components without additional connectors [13]. Fig. 1b shows a free-form full-scale prototype, which is a recent application of TT IMAs in spatial timber plate structures. Such structures are generally referred to as integrally-attached timber plate (IATP) structures.

The application of the IMA technique in timber plate structures has multiple advantages. It facilitates combining multiple simple-shaped planar timber plates to develop large-scale structures with complex geometries. The resurgence of elegant architectural design and construction of free-form structures has also been attributed to the use of IMAs in timber plates. Furthermore, prefabricated timber plates can be easily transported to the construction site and assembled without specialized workmanship and high labor costs. Moreover, during the design process, different structural typology and joint geometry can be generated, which, in particular, can optimize the force flow. This unique characteristic of IMAs can be used to optimize structural performance. Lastly, the use of IMAs improves the sustainability of timber construction since metal connectors are not used in the IATP structure.

1.2. Motivations and scope of the current study

Several recent studies have investigated different aspects of IATP structures, particularly (i) architectural geometry development and CAD (Fig. 2a) [14], (ii) digital fabrication, robotic assembly, and construction (Fig. 2b-c) [9,14,15], (iii) numerical modeling and structural simulation (Fig. 2h) [16–18,36], and (iv) physical experiments (Fig. 2d-g) [2,3,19,20]. These different modules have demonstrated the unique ability of IMAs to serve as the connections in spatial timber plate structures and their governing role in the overall response.

So far, the tensile, edgewise, and rotational behavior of TT IMAs have been widely investigated using physical experiments (Fig. 2d to f). However, to gain insight into the behavior of free-form IATP structures, it is necessary to also understand the flatwise behavior of the TT joints (Fig. 2g), which is the primary motivation of this paper. Because of their geometry, the flatwise behavior of the TT joints corresponds to the out-of-plane response of the IATP element in their joint region (hence the description of this behavior as out-of-plane response [4,20–22]). The kinematics of the flatwise behavior of TT joints in free-form IATP structures is detailed in Section 2.2.

The mechanical behavior of TT joints is characterized using well-known parameters, including the slip modulus (joint stiffness), ductility, yield and maximum strengths, and the corresponding deformations. The current study will shed light on the structural performance of IMAs and facilitate the development of design provisions, which are not present in modern building codes (e.g. Eurocode 5 [6]). Section 2 provides a brief overview of IATP structures. The assembly process used to interlock the timber plates is explained and the out-of-plane (flatwise) load-transfer mechanism is examined. Section 3 defines the design parameters of interest, specifies key assumptions, and documents the geometric characteristics of the test specimen groups. The loading protocol and test setup are described in Section 4. The results are discussed in Section 5, and the conclusions of the study are presented in Section 6.

2. Timber plate structures with wood-wood connections

2.1. Description of the system

Using TT joints, two timber elements are assembled only along the direction of the tab insertion angle, which restricts plate movements to a single translational vector. It is within this context that this method of assembly is described as a “one degree-of-freedom (1DOF)” joinery technique [2,3,21], which enables the sequential interlocking assembly of timber plates. The geometric optimization, fabrication and assembly of double-layered thin timber plate structures using 1DOF joinery is detailed in Robeller et al. [9]. In brief, the target surface of a free-form structure (Fig. 3a) is established by utilizing parametric geometric processing tools within a CAD platform. This target surface is then discretized into planar

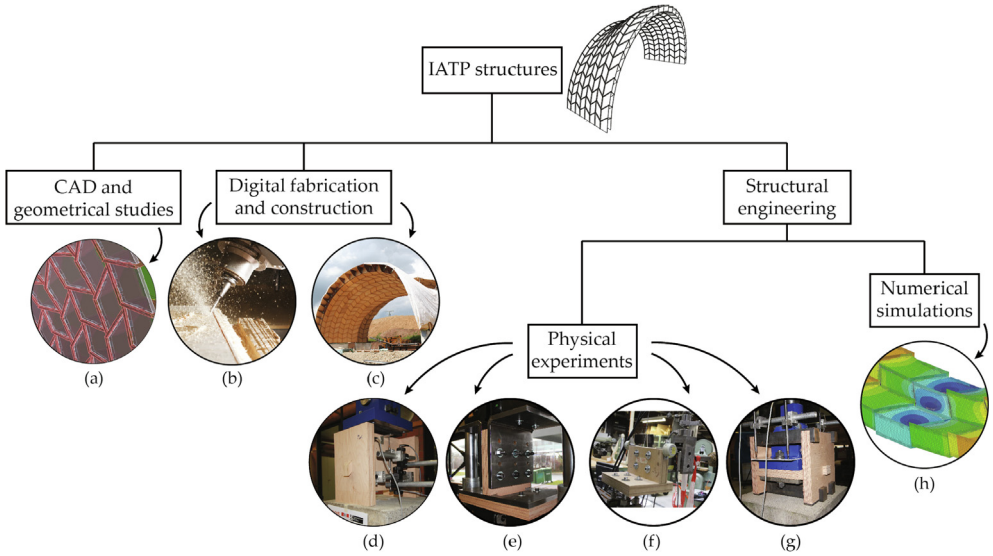

Fig. 2. Different modules involved in the development of IATP structures: (a) CAD framework, (b) digital fabrication, (c) construction, experiments to study the behavior of TT joints under (d) edgewise (in-plane), (e) tensile, (f) flexural and, (g) flatwise (out-of-plane) loads, and (h) numerical simulations.

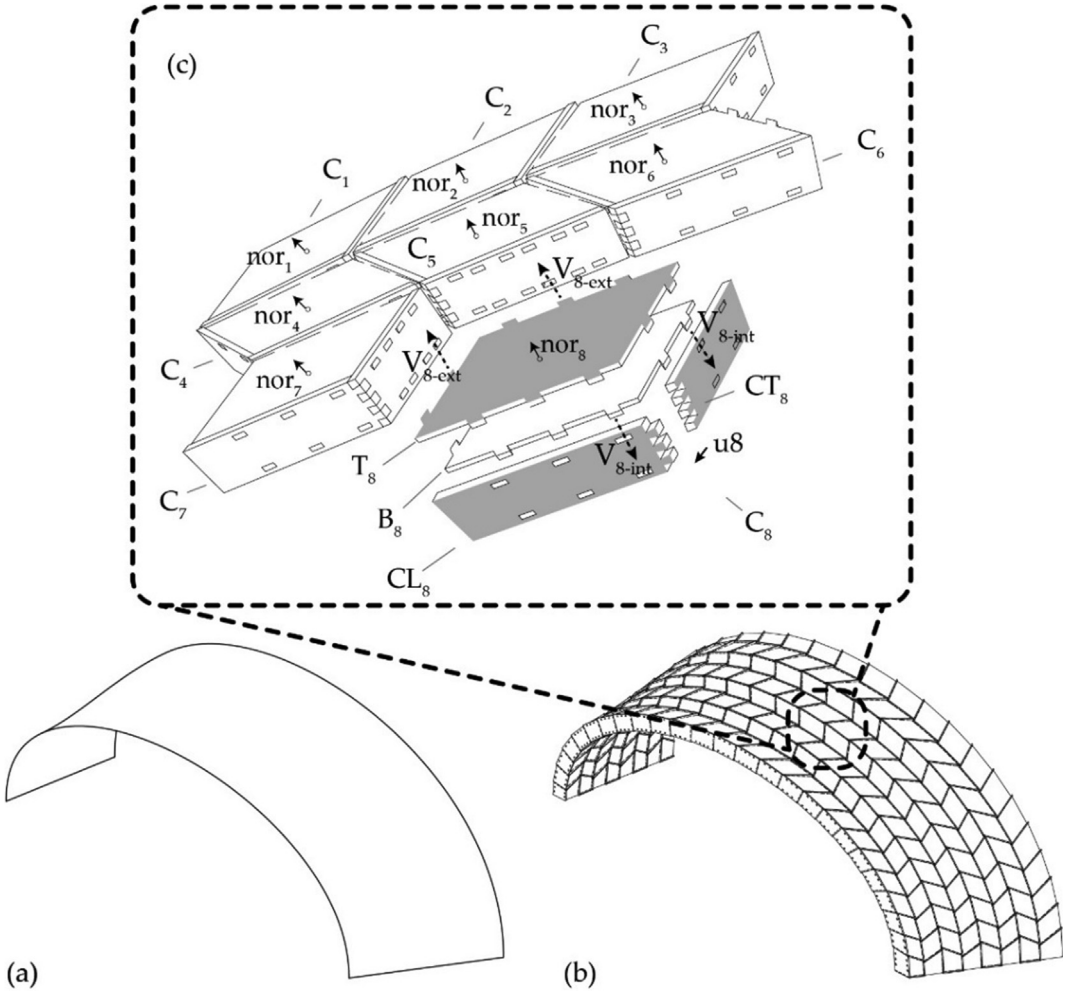

Fig. 3. Description of the IATP system: (a) the target surface associated with a free-form shape, (b) discretization of the target surface, and (c) the assembly process.

segments or "design patterns" (the latter term is used in digital architectural design). A unique vector normal to each planar surface is then established and two offset layers are specified in the corresponding direction. These two layers are identified as the

top plate, T_i, and bottom plate, B_i, in Fig. 3b-c, where i = 1, 2,...8. The T_i andB_i plates are then connected to the longitudinal and transverse cross plates, which are identified as CL_i and CT_i in Fig. 3c, respectively. Accordingly, the entire structural system is constructed through the assembly of several 4-sided boxes, where each box includesT_i, B_i, CL_i, and CT_i plates (each box is denoted as C_i in Fig. 3c). The T_i/B_i plates are connected to the CL_i/CT_i plates via the TT joints and along the insertion vector V_{i-int}, which is unique to each box. Furthermore, dovetail joints connect the CL_i and CT_i plates along the assembly vector, u_i (Fig. 3c). Each box is then connected to the neighboring boxes along the vector V_{i-ext}. This is illustrated in Fig. 3c, which shows C_8 being simultaneously connected to C_5 and C_7 along the vector $V_{8,ext}$. This assembly process leads to full contact between the edges of neighboring plates, which, in turn, allows the structural system to benefit from the form/geometry and optimize the force flow.

2.2. The flatwise (out-of-plane) force-flow mechanism

The kinematic degrees of freedom (DOFs) associated with the 3D continuum geometry of the joint region is idealized using a two-node link element according to Nguyen et al. [16] and Rezaei Rad et al. [2,3]. The link element consists of six different springs, which capture the tensile, in-plane (edgewise) and out-of-plane (flatwise) force–deformation, and flexural, and torsional moment-rotation behavior of the joint region. Fig. 4a shows the joint region and the equivalent spring elements.

The load-carrying mechanism under out-of-plane (flatwise) loads is described for those TT joints that are used in free-form IATP structures. Referring to Fig. 4b-c, $Vec_{i,int}$ and $Vec_{i,ext}$ denote the insertion vectors associated with the intra- and inter-box assembly, respectively. Defining x', y' and z' as the local coordinate system (LCS) for the T_i plate that belongs to C_i, it follows that $u_{z'}$ and $u_{C\,i,z'}$ are the direction of the out-of-plane load imposed on the intra- and inter-box TT joints, respectively. The direction of the out-of-plane load is along the local z' axis, which is perpendicular to the local x′y′ plane. Considering the equivalent spring element (Fig. 4a), DOF #3 represents the response of the TT joint under this loading condition. In other words, DOF #3 aims to represent the relative (translational) load-deformation of the joint region along the local z' axis. It is worth noting that the tensile [2] and edgewise (in-plane) [3] behavior of the TT joints, which are represented by DOF #1 and DOF #2 in the equivalent spring element, are located in the local x'y' plane. Out-of-plane loads can potentially give rise to multiple resisting mechanisms (e.g. embedment, compression perpendicular to fibers, shear, etc.), each of which is investigated in the current study.

3. Description of test specimens

BauBuche beech LVL timber boards with 40 mm thickness, which were used in the building-scale prototypes (Fig. 1b), are utilized in the experiments. The mechanical properties of BauBuche beech LVL, which is a hardwood material manufactured by Pollmeier [22], are specified in Table 1.

Two design parameters are varied in the experiments: (i) the tab insertion angle, and (ii) the fiber orientation. Three tab insertion angles, 45°, 60°, and 90°, are considered. The range of this parameter is constrained by the fabrication process based on the permissible degree of rotation in the 5-axis CNC machine. Specifically, the CNC machine cannot rotate more than 45° in the process of milling the timber board. Furthermore, 60°-angled tenons were mainly used in the full-scale prototypes. Therefore, these three tab angles reasonably capture the range of possible insertion paths. Two categories of fiber orientation are adopted for the test specimens. The first category includes eleven cross-wise and two longitudinal fiber layers over the tenon cross section (cross-plies ratio = 11/13). The fibers in the second category are oriented 90° with respect to those in the first category i.e. eleven longitudinal and two cross-wise fiber layers (cross-plies ratio = 2/13). Fig. 5 shows the distribution and configuration of the fiber layers for the two categories. Considering the aforementioned two design parameters and their ranges/categories, six specimens were designed and fabricated. Furthermore, six replicates were tested for each specimen. Table 2 summarizes the properties of each type of specimen.

The TT joint dimensions, including the height, width, and length of the tenon and slot components, which are generated using algo-

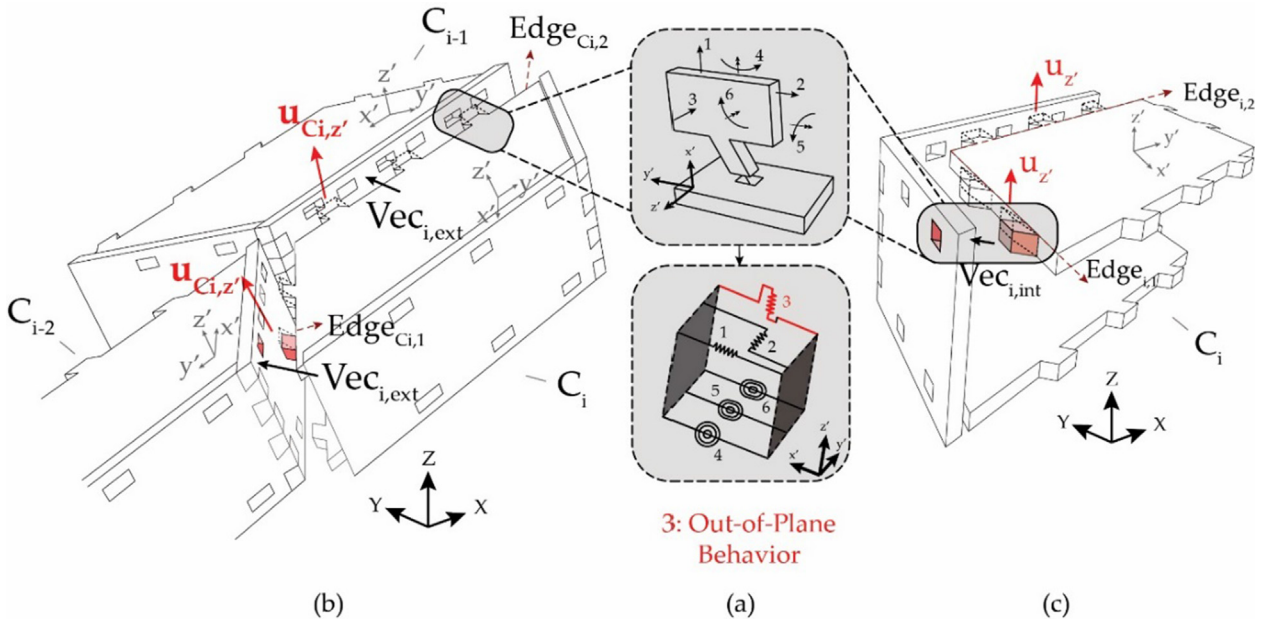

Fig. 4. (a) Discrete spring representation of a TT joint, and identification of the out-of-plane (flatwise) DOF. The direction of the flatwise behavior in the (b) intra-box TT joints and (c) inter-box TT joints.

Table 1
Mechanical properties of 40 mm thick BauBuche beech-Q s [4].

Symbol	Description *Mean Modulus*	Value	Symbol	Description *Mean Strength*	Value	Symbol	Description *Mean Strength*	Value
E_0	Modulus of elasticity, 0°	13200.	$f_{m,0}$	Edgewise Bending, 0°	60.	$f_{t,0,k}$	Tension, 0°	51.
E_{90}	Modulus of elasticity, 90°	2200.	$f_{m,90}$	Edgewise Bending, 90°	10.	$f_{t,90,k}$	Tension, 90°	8.
G_0	Shear modulus, 0°	820.	$f_{c,0,k}$	Compression, 0°	53.3	$f_{v,0,k}$	Edgewise Shear, 0°	7.8
G_0	Shear modulus, 90°	430.	$f_{c,90,k}$	Compression, 90°	19.	$f_{v9,0,k}$	Edgewise Shear, 90°	3.8

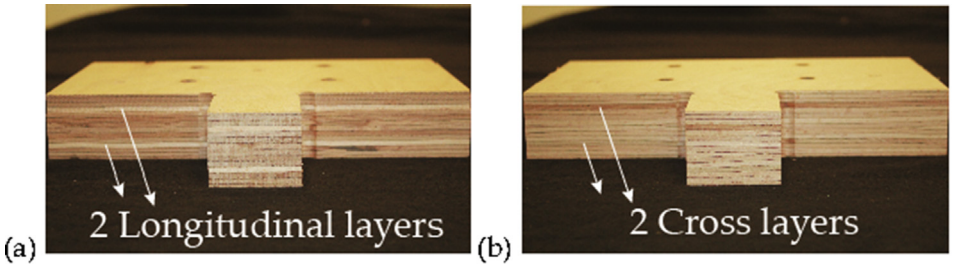

Fig. 5. Cross section of tenon with (a) 11 cross-wise and two longitudinal layers of fiber, and (b) 11 longitudinal and two cross layers of fiber.

Table 2
Summary of test specimens.

Timber Material	LVL Beech-Q, 40 mm					
Fiber Orientation	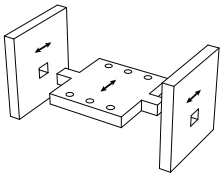			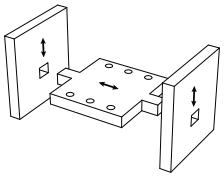		
Insertion Angle (°)	45	60	90	45	60	90
Group ID	T1	T2	T3	T4	T5	T6

rithmic geometric processing, are shown in Fig. 6. Depending on the design load, a broad range of geometric configurations and dimensions can potentially exist. Nevertheless, in the current experiments, the joint geometry was derived from the average dimension of the joints used in the physical prototype (Fig. 1b). Moreover, the adopted joint dimensions are consistent with the values used in previous studies (see [2,3]).

4. Experimental methodology

4.1. Specimen design and test setup

The test setup adopted by the Structural Engineering Laboratory at École Polytechnique Fédérale de Lausanne (EPFL) was designed

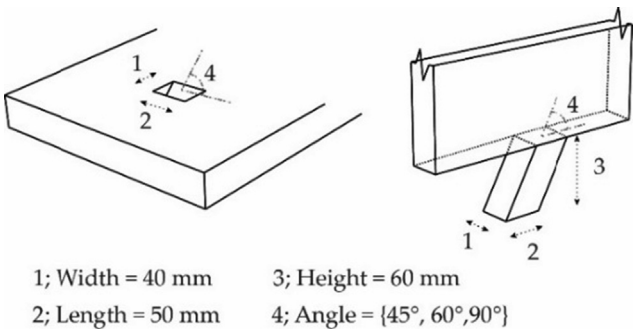

Fig. 6. Dimensions of a single tenon and slot component.

to isolate the flatwise (out-of-plane) force–deformation response of the TT joint region. To minimize undesirable effects and unwanted loading and response conditions, a symmetric configuration was adopted. More specifically, each test specimen included two tenons, and consequently, two slots (Fig. 7). The tenons were fabricated in one timber plate, and the slots were fabricated in two separate plates. After assembling the tenon and slot elements, the vertical plates with the slot components were placed on top of a rigid concrete base and the force was applied to the horizontal plate with the tenon component. Using this configuration aligned the center of rigidity of the specimen with the vector that is oriented along the flatwise load. Fig. 7 shows the geometry of a typical specimen and steel supports, the associated dimensions, and the test setup. Four Linear Variable Differential Transducers (LVDTs), supported at the ground, were attached to the specimen at the corners of the horizontal plate. The LVDTs were used to measure the relative displacement between the slots and tenons. The exact position of the LVDT is shown in Fig. 7d. Using LVDTs at the four corners enabled an evaluation of any torsional response, which is discussed in Section 5.1. A 300 kN hydraulic jack with a maximum stroke of 100 mm was used to apply a surface load to the horizontal timber plate. The area loaded by the hydraulic jack is 300 mm × 240 mm and highlighted in orange in Fig. 7d.

Steel supports (Fig. 7f, g) were employed at the top and bottom of each test specimen to ensure that the two vertical plates remain plumb during loading and to avoid lateral displacement. In other words, the steel supports were used to prevent the test specimens from bending, which is an unwanted loading condition for this experiment. Additionally, a rectangular-shaped steel plate

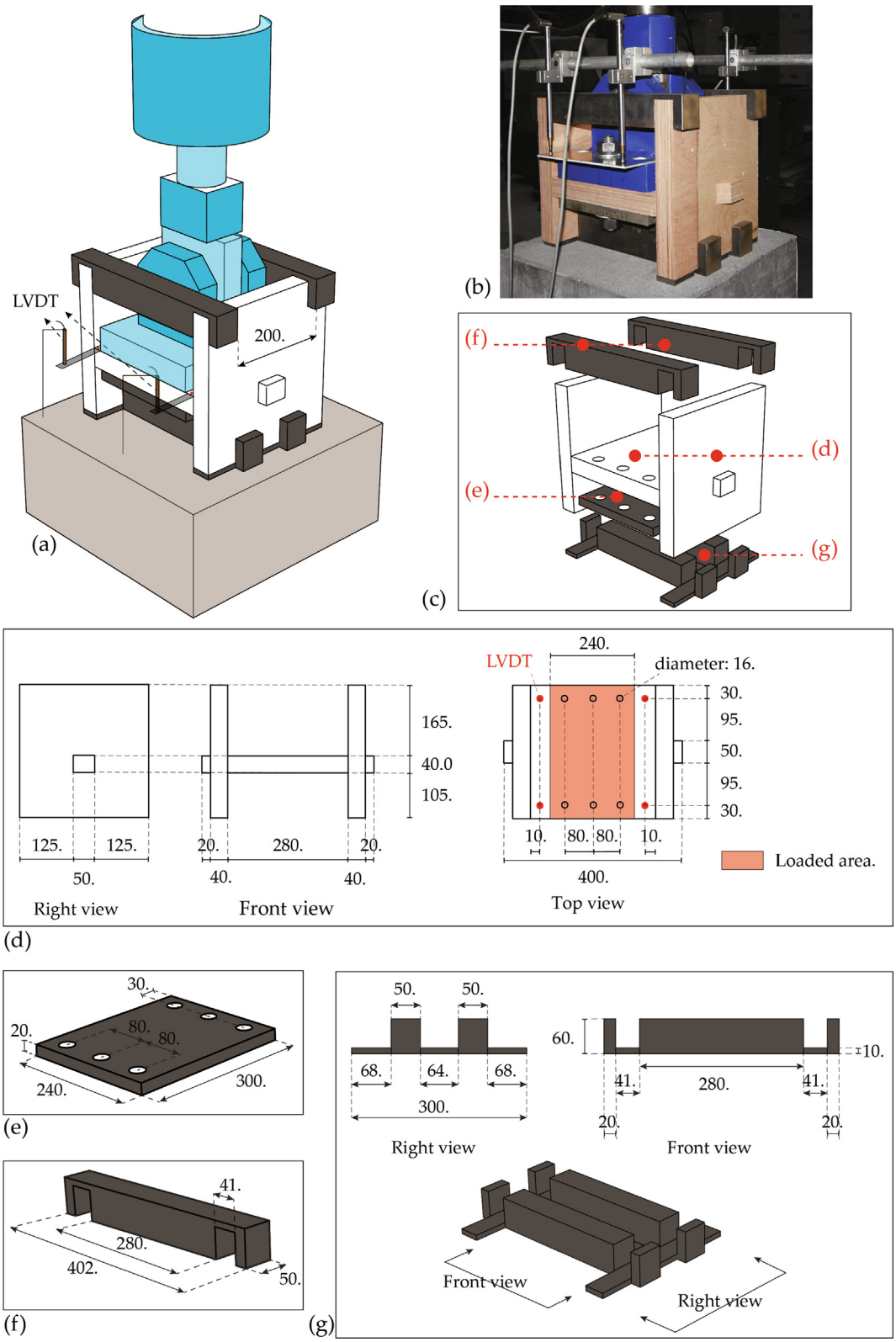

Fig. 7. (a-b) The experimental setup used for the flatwise test, (c) components of the test setup, including two through-tenon joints and steel supports, (d) dimensions (in mm) of the through-tenon joints, (e) dimensions of the steel plate attached to the tenon, (f) dimensions of the steel supports attached to the top of the slots, (g) dimensions of the steel support attached to the bottom of the slots.

(Fig. 7e) was attached to the bottom surface of the horizontal plate to prevent bending and ensure a uniform distribution of the out-of-plane load. By utilizing these various steel supports, the translational flatwise behavior of the TT IMAs was isolated, and the focus was placed on the interaction between the tenon and slot along the out-of-plane direction of the horizontal plate. Consequently, the TT

joints were loaded normal to the local x'y' plane (see Fig. 4 for the local axes). As a result, the relative translational load–displacement response between the tenons and slots was measured and assigned to the discrete spring elements shown in Fig. 4a.

4.2. Experimental loading procedure

The European Committee for Standardization (CEN) loading protocol for timber joints, EN 26891 [23], was used in the experiments. This testing procedure relies on an estimation of the maximum strength of the specimen, F_{Max}. Therefore, prior to the start of the loading, F_{Max} was determined by testing a dummy specimen. Overall, the loading protocol begins with a force-control phase, where the specimens are loaded to 40% F_{Max}. After a 30-second pause, the load is reduced to 10% F_{Max}, which is maintained for another 30 s. In the last part of the force-control phase, the load is increased to 70% F_{Max}. It is worth noting that the first and last step of the force-control phase correspond to the Serviceability (SLS) and Ultimate (ULS) Limit State, respectively [24]. The loading procedure is then followed by a displacement-control excursion with the same loading rate used in the force-control phase. The overall loading protocol is illustrated in Fig. 8. Utilizing EN 26891 [23], the mechanical properties of the joint, including the stiffness, ductility, strength, and design deformations are determined and reported in Section 5. Furthermore, because of the loading–unloading process in the early phase of the protocol, full interlocking contact between the slot and tenon components is achieved during the test. Consequently, the fabrication variabilities caused by the CNC robots were considerably reduced.

5. Results and discussions

Qualitative and quantitative evaluations of the observed load-deformation behavior of the TT joints are provided in this section. The qualitative assessment (Section 5.1) includes descriptions of the failure modes and various load resisting mechanisms. Using the European standards EN 26891 [23] and EN 12512 [25], the quantitative performance evaluation (Section 5.2) describes the joint strength and associated deformation at yield, maximum and ultimate states, stiffness, ductility demand, and the design strength and deformations associated with the SLS and ULS. The European standards are chosen over the other alternatives (i.e. EEEP Method [26], 0.5-FMAX Method [27], and 10-40-50 Method [28]) because: (i) they have been verified and well integrated into the performance evaluation of IMAs as it has been shown in Roche et al. [5], Roche [7], and Milch et al. [29], and (ii) they are consistent with the loading procedure (Section 4.2).

5.1. Qualitative evaluation: force–deformation response

The force–deformation response of specimens T1 to T3, where most of the fibers are oriented perpendicular to the loading direction (fiber-perpendicular specimens) (cross-plies ratio = 11/13), and T4 to T6, where most of the fibers are oriented parallel to the loading direction (fiber-parallel specimens) (cross-plies ratio = 2/13), are shown in Figure 9 and 10, respectively. Minimal replicate-to-replicate variability is observed for each specimen group during the pre-peak response. Furthermore, using the steel supports in the test setup, the relative rotation between the vertical and horizontal timber elements is restrained. Therefore, the load-deformation curves represent the translational flatwise behavior of the TT joints. Given this consideration, failure mechanisms caused by the flexural interaction between the tenons and slots are avoided. Instead, the test setup ensures that the observed failure modes are associated with the relative translational behavior of the TT joints. This, in particular, changes the joint capacity, however, it has not been studied in the current investigation and should be examined in the future.

The performance of the joints was deemed to be governed by (1) the tab (tenon) insertion angle, (2) the fiber orientation, and (3) the size of notches. The first two parameters were identified in Section 3, Table 1. The last parameter is a function of the tab insertion angle and the fabrication process. More specifically, to fabricate the TT joints, the fabrication contours are first generated and the G-code is then prepared so that the CNC robot can follow those contours to cut the timber board. The robot then rotates the tool used to mill the tenon component, which creates a notch. Figure 11 shows different notch sizes, which vary depending on the tab insertion angle and diameter of the fabrication tool. Using the same fabrication tool, the largest and smallest notch size was produced in the 45°and 90°-angled specimens, respectively.

The load-transfer mechanism and the failure modes for the fiber-perpendicular specimens (T1 to T3) were different from the ones observed in the fiber-parallel specimens (T4 to T6). This observation is attributed to the arrangement of the fibers over the cross section of the tenon components. In fact, the main fibers in the tenons of T1 to T3 are crosswise oriented. As noted earlier, in this case, the cross section consists of 11 cross layers and two longitudinal fiber layers (Fig. 5a). In other words, the main fiber direction is oriented perpendicular to the loading direction. Prior studies have shown that the timber fibers exhibit superior performance (high strength/stiffness/ductility) when they are oriented

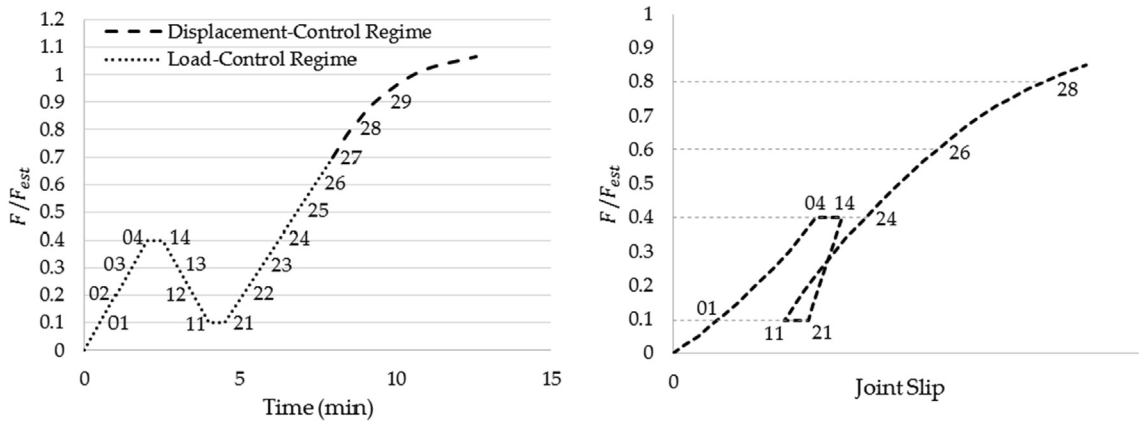

Fig. 8. The loading protocol specified in EN 26891 [23].

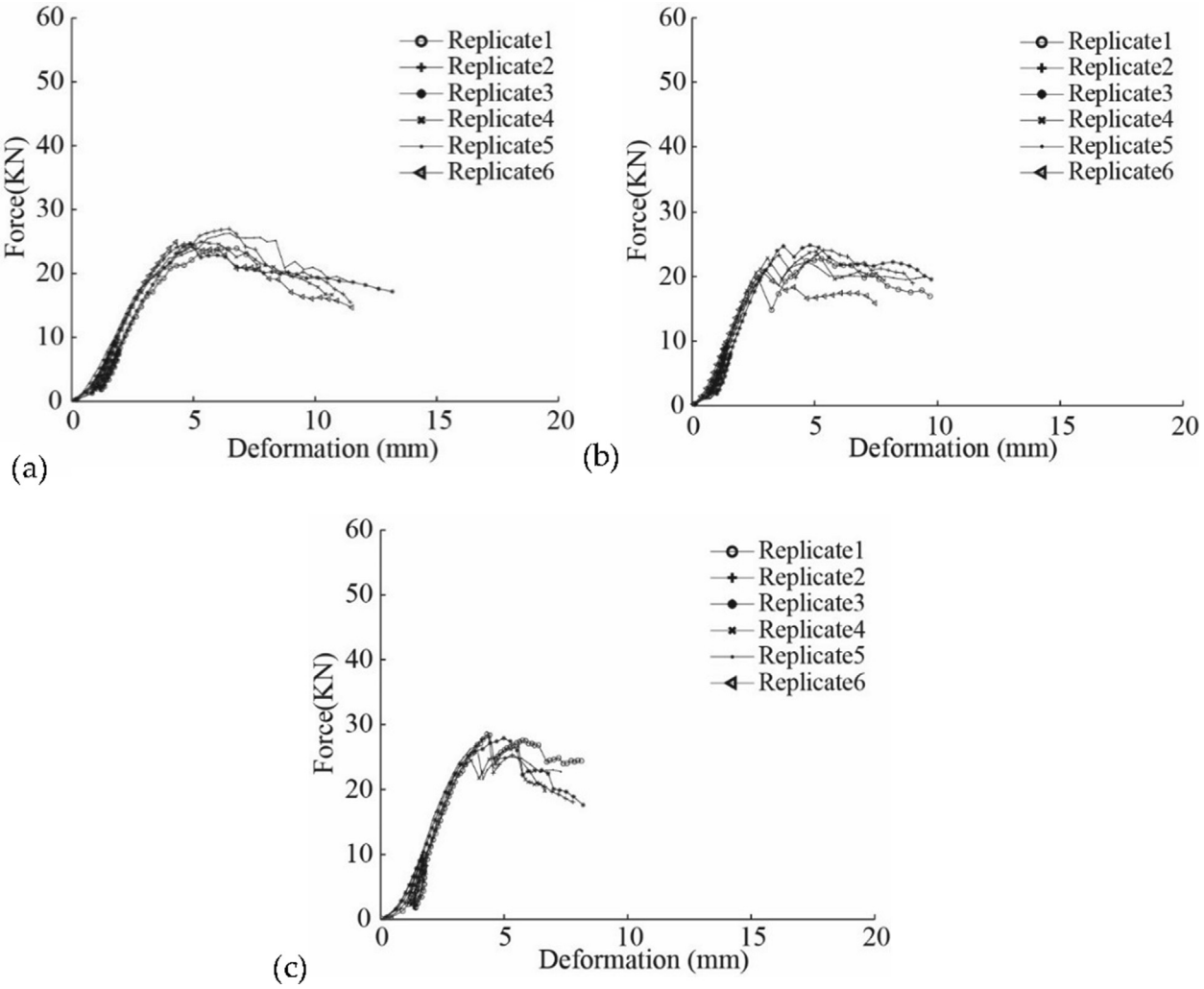

Fig. 9. Out-of-plane force–deformation curves for fiber-perpendicular specimens (a) T1, (b) T2, (c) T3.

parallel to the load direction [2,3,7]. This is consistent with the low strength and brittle failure mode observed in specimens T1 to T3, where the load is transferred between the tenon and its mate, creating a shearing mechanism between the fibers. In fact, the cellular walls between the fibers (hereafter described as the inter-fiber layers) provide the bulk of the resistance. Referring to Table 1, the shear capacity is very low in this type of configuration (only 3.8 MPa) and consequently, the fiber-perpendicular joints ruptured in a brittle manner. Fig. 12 shows the schematic representation and the actual failure mode in this case. The two longitudinal layers, which are shown in Fig. 12, resisted most of the load, while the cross layers provided minimal resistance. The rupture surface was located at the beginning of the tenon at the interface with the slot (see Fig. 12).

For the fiber-parallel specimens (T4 to T6), the cross section consists of 11 longitudinal and two crosswise layers (Fig. 5b). In other words, the main fiber orientation of the cross section is parallel to the loading direction. As such, the out-of-plane load was transmitted from the tenon to the slot through the following resisting mechanisms: (1) fiber tension–compression and flexural resistance, (2) embedment compression resistance, (3) inter-fiber layer resistance, (4) fiber torsional resistance, and (5) fiber shear resistance. The extent to which each mechanism contributes to the overall resistance depends on the tab insertion angle and the notch size. For all fiber-parallel specimens, the tenon acts like a beam on elastic foundation element. As such, the fiber tension–compression and flexural resistance are activated (see A-A-1 and A-A-2 for the bending resistance, and B-B-1 and C—C—1 for the tension–compression resistance in Fig. 13). Furthermore, because of the interaction between the tenon and slot, the embedment compression resistance is activated in these specimens (see B-B-2 in Fig. 13). Tenons with an insertion angle of 90° create a symmetric geometry and thus, the TT joint is subjected to minimal torsional demands. On the other hand, asymmetric joints such as those with a 45° or 60° insertion angle can potentially activate the inter-fiber layer (see C—C—2 in Fig. 13), torsional (see C—C—3 Fig. 13), and shear resistances of the tenon (see C—C—4 in Fig. 13). It was also observed that the rate of damage was slower in the T4 to T6 specimens compared to T1 to T3. Furthermore, the damage in the former was not concentrated in a specific location/surface but distributed in different regions around the tenon.

The steel piece attached to the vertical timber plates (Fig. 7g) provides a continuous support for the test specimen. During and after the experiments, no sign of embedment deformation or crushing was observed at the support area of the vertical plates. This is mainly attributed to the high compressive strength of beech LVL, as well as the continuous and uniform contact area established between the vertical timber plates and the steel. Furthermore, the contact length between the tenon and mortise (Fig. 6) is one-sixth the contact length between the vertical timber plate

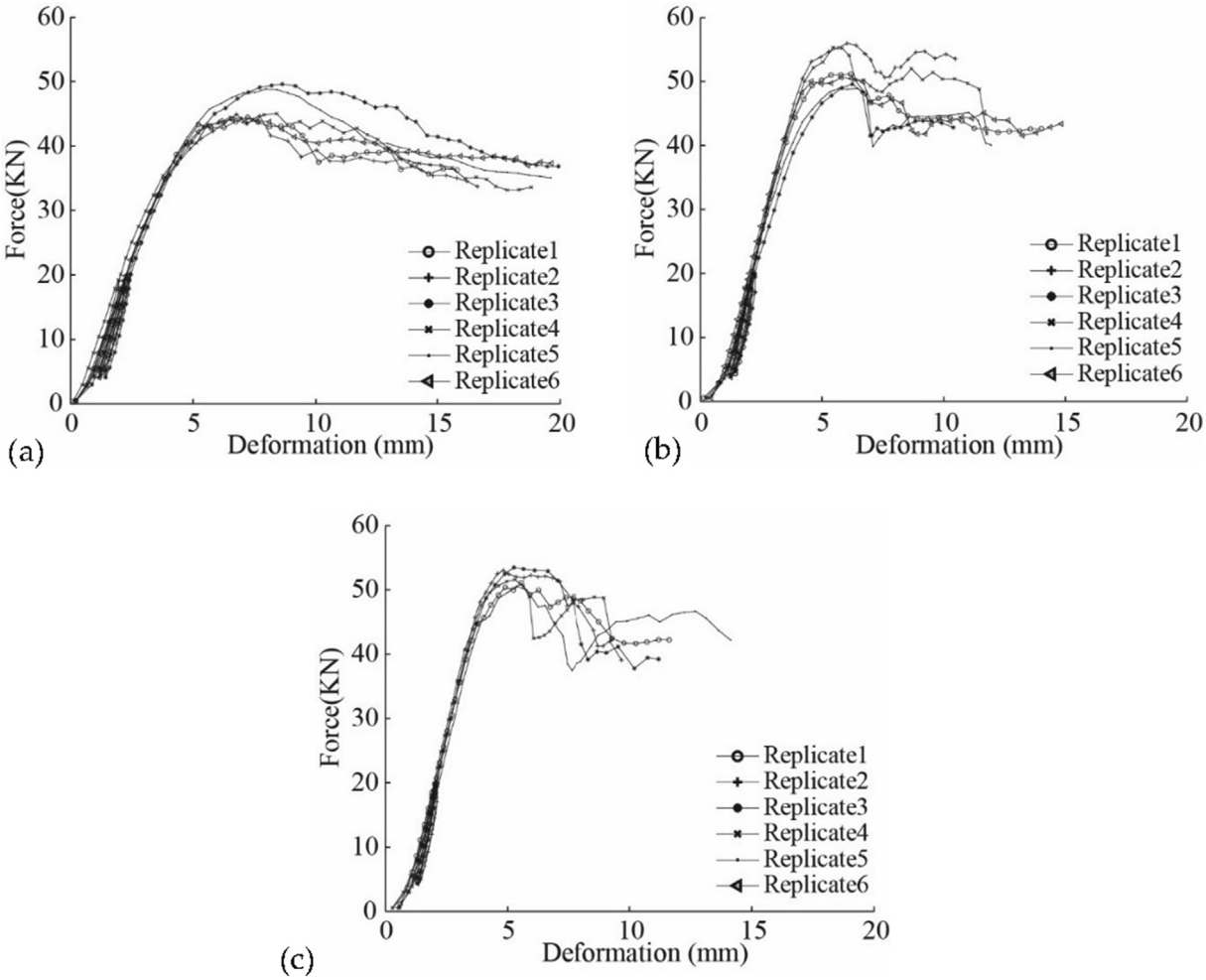

Fig. 10. Out-of-plane force–deformation curves for fiber-parallel specimens (a) T4, (b) T5, (c) T6.

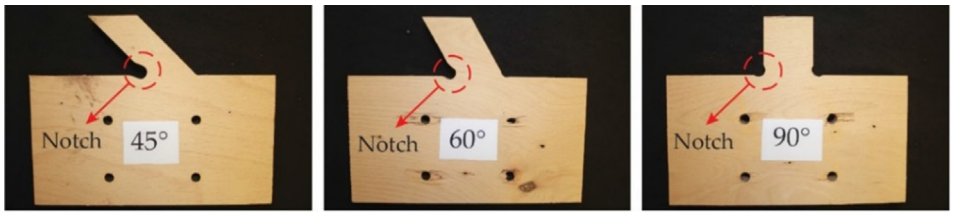

Fig. 11. The effect of fabrication on the notch size in tenon components.

and the steel support (Fig. 7g). Accordingly, it is assumed that the contact area between the vertical timber element and the lower steel support did not contribute significantly to the overall load-deformation response. However, this contribution might be pronounced when softwood material is used.

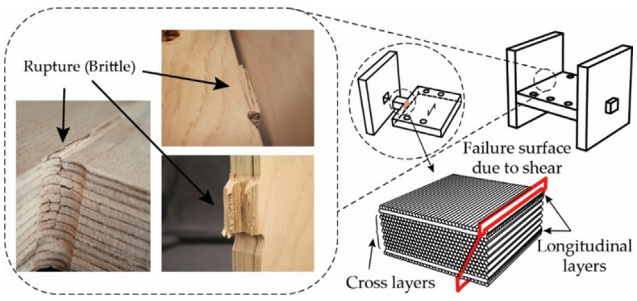

Fig. 12. Schematic representation and observed shear rupture failure mode in the fiber-perpendicular TT joints subjected to out-of-plane loading.

5.2. Quantitative performance assessment

The behavior of the joints is characterized using the design parameters specified in the European Standards for timber joints, EN 12512 [25] and EN 26891 [23], which identify three key points along the force–deformation curve: the yield and maximum strength and the ultimate limit state. Accordingly, the yield force (F_y) and deformation (D_y), the maximum force in the joints (F_{max}) and the corresponding deformation ($D_{F\text{-}Max}$), the joint stiffness (slip modulus) (K_s), ultimate deformation (D_u), and ductility capacity (μ), are computed from the experimental results. Using the CEN-1/6 method [25], the design parameters are schematically shown

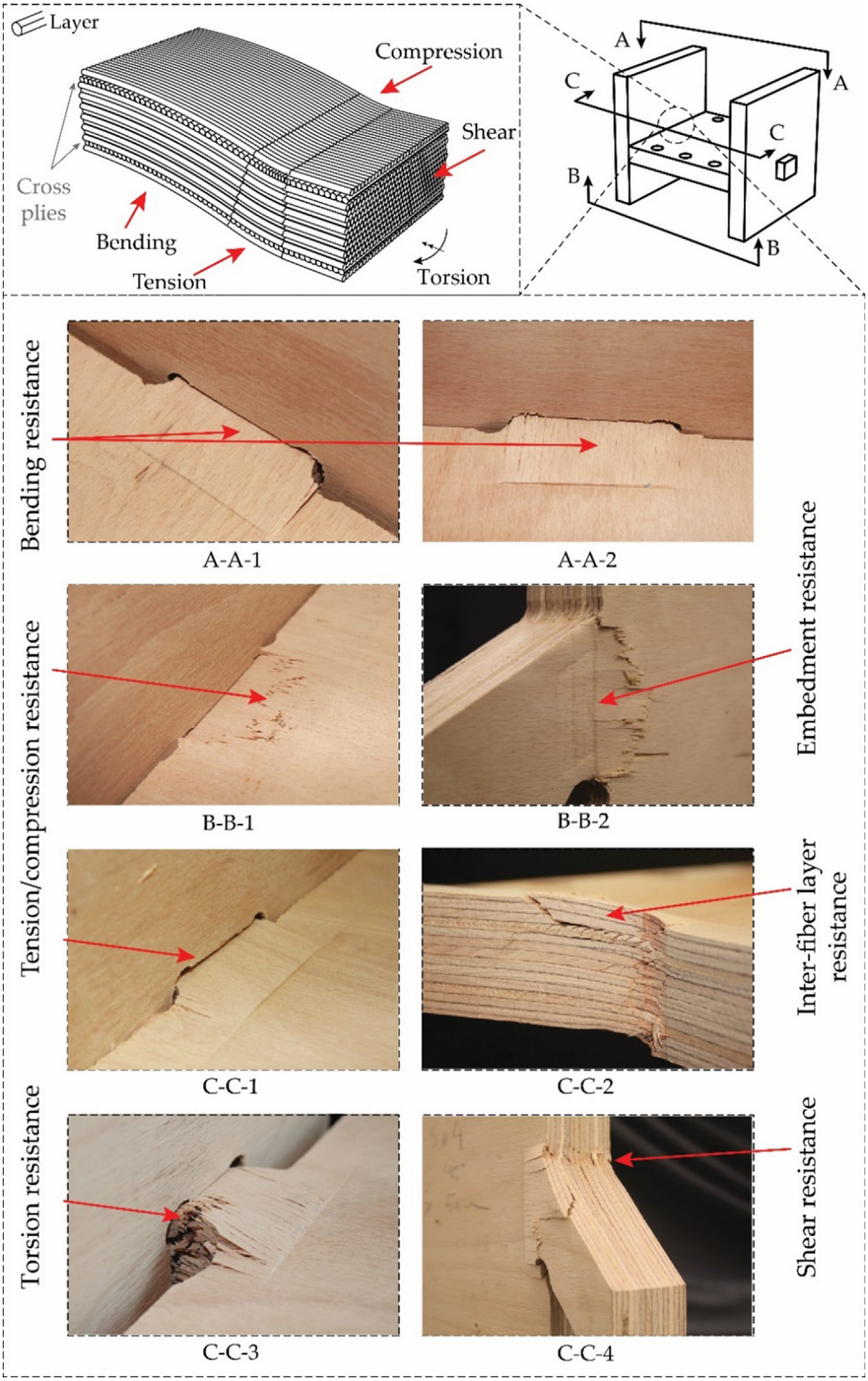

Fig. 13. Schematic representation and observed failure mode of the fiber-parallel specimens subjected to the out-of-plane load.

in Fig. 14a. The slip modulus and ductility capacity, which are widely used in the design of timber joints, are provided in Table 3. Furthermore, a multi-linear backbone curve, which is developed using the yield, maximum strength, and ultimate state points, is proposed for each specimen group. A schematic representation of the backbone curve is shown (in red) in Fig. 14a. This curve can be viewed as an idealization of the actual load-deformation response, and encapsulates the key design parameters for TT joints. Using the idealized curve, nonlinear performance assessment of IATPs is also possible. Given the four LVDT measurements (Fig. 7d), the mean force–deformation response and the associated backbone curve for each specimen group is shown in Fig. 14b-c (in gray and red, respectively).

The strength of the joints and associated deformation at the SLS and ULS are summarized in Table 3. The evaluation of the joint performance, especially at the SLS, is affected by age-related and non-

Table 3
Summary of design parameters for the specimens.

Group ID	T1		T2		T3		T4		T5		T6	
Strength (EN 26891) (KN)	SLS	ULS	SLS	ULS	SLS	ULS	SLS	ULS	SLS	ULS	SLS	ULS
[COV]	4.98	8.73	4.48	7.84	5.28	9.24	9.23	16.15	10.5	18.38	10.38	18.17
	[0.04]	[0.04]	[0.06]	[0.06]	[0.02]	[0.02]	[0.05]	[0.05]	[0.05]	[0.06]	[0.02]	[0.02]
Deformation (EN 26891) (mm)	SLS	ULS	SLS	ULS	SLS	ULS	SLS	ULS	SLS	ULS	SLS	ULS
[COV]	1.95	2.12	1.43	2.13	1.85	2.61	2.12	3.54	2.18	3.28	2.12	3.07
	[0.07]	[0.05]	[0.10]	[0.09]	[0.06]	[0.05]	[0.09]	[0.07]	[0.04]	[0.04]	[0.03]	[0.02]
Ductility (EN 12512) [COV]	2.85		2.64		2.19		4.04		2.94		2.44	
	[0.13]		[0.31]		[0.27]		[0.14]		[0.21]		[0.28]	
Slip Modulus (EN 26891) (KN/mm) [COV]	3.53		4.21		4.16		5.47		7.17		7.43	
	[0.05]		[0.03]		[0.08]		[0.01]		[0.05]		[0.08]	

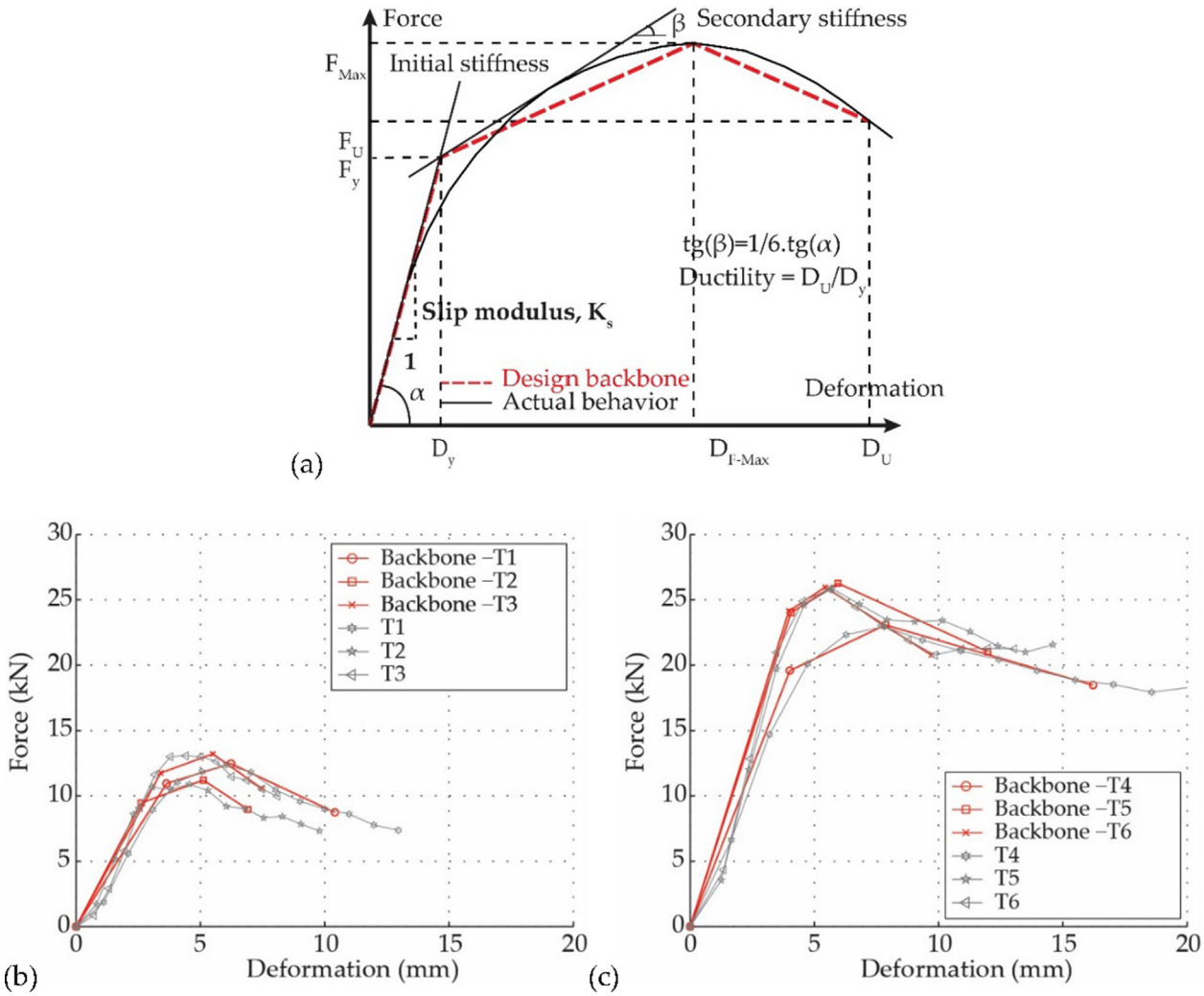

Fig. 14. (a) Definition of the design parameters (CEN-1/6-method [25] is used for ductility) and mean force–deformation and corresponding backbones curves for (b) fiber-perpendicular and (c) fiber-parallel specimens.

age-related parameters. The propensity for creep, cyclic loading history, moisture content, and the roughness of the contact surface are examples of age-related parameters. The tool size and associated notches around the tenons, fabrication imperfection, interlocking state, and the surface-to-surface contact pressure that occurs during the assembly are non-age-related parameters. Using the EN 26891 loading procedure, the aim is to quantitatively measure the instantaneous mechanical properties of the joints without considering age-effects. However, it is noted that the increase in initial slip over time is not considered in the quantitative performance assessment.

5.2.1. Strength and stiffness of the joints

5.2.1.1. Yield strength. The EN 12512 standard [25] is used to determine the yield point of the TT joints. Accordingly, the pre-peak force–deformation response is idealized into two linear parts: (a) the first line crosses 0.1* F_{max} and 0.4* F_{max}, and (b) the second line crosses the maximum strength with the slope corresponding to 1/6

that of the first line. As shown in Fig. 14a, the yield point is then identified as the intersection of these two lines. For T1 to T3, the yield strength is almost independent of the tab insertion angle, ranging between 9.5 kN and 11.7 kN. The minimal influence of the tab insertion angle on the yield strength is mainly attributed to the configuration/arrangement of the fiber layers over the cross section of the tenon component (see Fig. 5 for the configuration). As noted earlier, most of the fiber layers of the tenon are crosswise oriented for T1 to T3 and provide little resistance. Accordingly, the behavior is controlled by the resistance of the inter-fiber layers, which is a function of the wood cellular structure (Fig. 12). At the microscopic scale, the resistance of the inter-fiber layer depends on the thickness of the cellular walls of the wood material [30]. For beech LVL, the thickness of these cellular walls is almost constant over each layer. Therefore, the yield strength of the joints remains almost unchanged even when the tab insertion angle is varied (Fig. 15a).

For T4 to T6, where 11 fiber layers are longitudinally oriented (see Fig. 5b for the configuration), the yield strength is considerably higher than that of the T1 to T3 specimens. It is also observed that the notch size has a strong influence on the performance of the T4 to T6 specimens because the effective cross sectional area of the tenons is reduced. For the specimens with a 45° tab insertion angle (T4), the notch reduced the cross sectional area by almost 17%. Whereas, for the 60°- and 90°-insertion angle specimens (T5 and T6), the notch reduced the cross sectional area by 4% and 2%, respectively (Fig. 11). As such, the T4 specimens have the lowest yield strength. The T5 and T6 specimens have approximately the same yield strength because of their similar notch sizes (Fig. 15a). It is worth noting that the role of the notch size is only significant in specimens T4 to T6. In fact, the arrangement of the fiber orientation in these specimens activates different load-transfer mechanisms, namely, flexural, tension–compression, embedment, and torsion, which are primarily controlled by the cross section size.

5.2.1.2. Maximum strength. The maximum strength of the specimens in the different groups is compared in Fig. 15b where the F_{max}/F_y ratio is also introduced. For all specimens, F_{max}/F_y is near or equal to unity (Fig. 15a), which means that the maximum strength is reached soon after yielding. In other words, regardless of the fiber orientation and insertion angle, the damage that is initiated at the yield point quickly propagates throughout the cross section resulting in very little pre-peak nonlinear behavior. This finding is consistent with the nature of wood material, which is known to be brittle [31,32]. The other implication is that the aforementioned observations regarding the yield strength also apply to the maximum strength, which is almost constant among the T1 to T3 and T4 to T6 specimens.

5.2.1.3. Joint stiffness (slip modulus). The joint stiffness is computed using the procedure specified in European Standard EN 26891 [23]. Informed by the experiments, the joint stiffness for each specimen is computed using Eq. (1) and shown in Fig. 16.

$$K_s = 0.4 * \frac{F_{est}}{\upsilon_{i,mod}} \tag{1}$$

where F_{est} is the estimated maximum force ($F_{est} = F_{Max}$), and $\upsilon_{i,mod}$ is the modified initial slip (Eq. (2)).

$$\upsilon_{i,mod} = \frac{4}{3}(\upsilon_{04} - \upsilon_{01}) \tag{2}$$

where υ_{01} and υ_{04} are the amount of slip at the first and fourth loading steps (see Fig. 8a).

For all specimens, $\upsilon_{i,mod}$ was found to be approximately 1.25 mm. Therefore, and according to Eq. (1), the joint stiffness is directly proportional to F_{max}. Since F_{max} is approximately the same for T1 to T3, the associated joint stiffness was minimally influenced by differences in the tab insertion angle. However, among the T4 to T6 specimens, the joint stiffness of the 45°-angled specimens (T4)

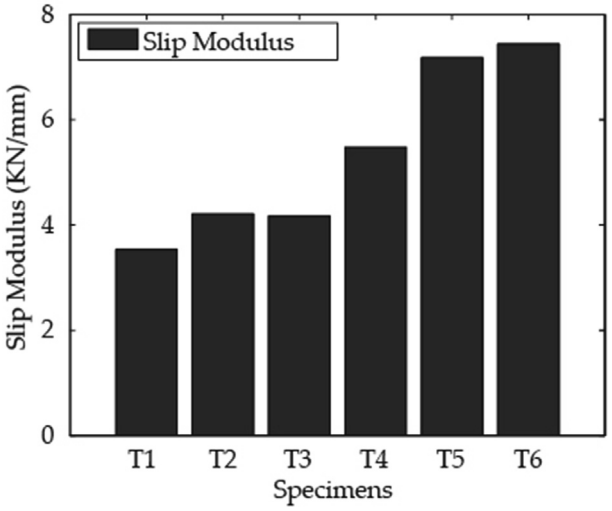

Fig. 16. Joint stiffness (slip modulus).

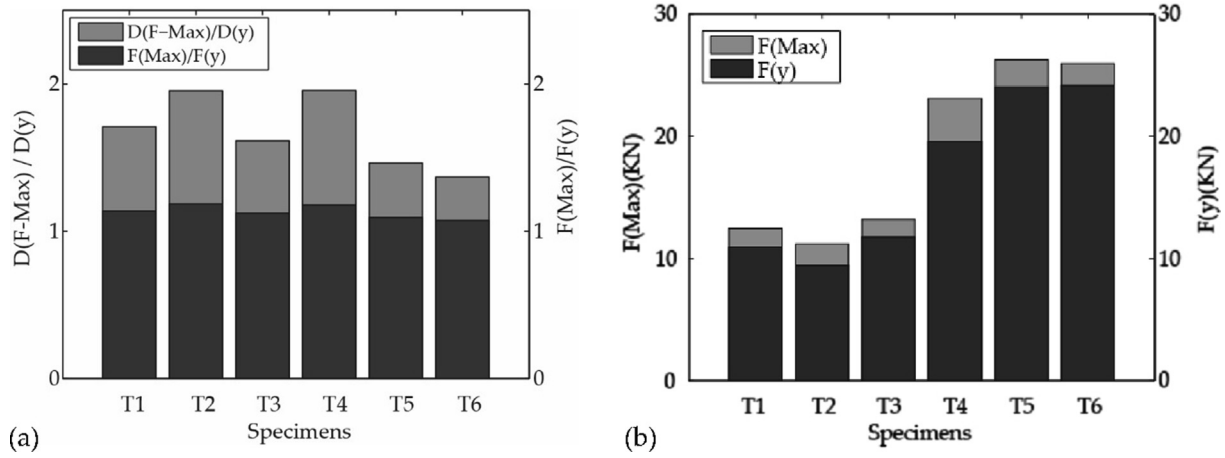

Fig. 15. Maximum and yield deformation and force of the TT joints.

was less than that of the 60° (T5) and 90°-angled (T6) specimens. The lower F_{max} in T4 explains this observation. Furthermore, because T5 and T6 have similar F_{max} values, their stiffnesses are approximately the same. Another key finding is that the joint stiffness for specimens T4 to T6 is greater than that of T1 to T3. This is explained by the orientation of the fibers over the cross section (see Fig. 5 for the fiber orientation), which makes T1 to T3 weaker and more susceptible to rapid damage propagation.

5.2.2. Deformation at yield and maximum strength

For T1 to T3, it was observed in Section 5.2.1 that (i) the inter-fiber layer resistance, which is provided by the wood cellular walls at the microscopic scale, governs the pre-peak behavior, and (ii) the TT joints exhibit almost linear elastic behavior between the yield and maximum strength. It therefore follows that the pre-peak force–deformation response is almost linear for T1 to T3. Therefore, a linear relationship exists between the strength and deformation properties. As such, the findings related to the yield strength described in Section 5.2.1, also apply to the associated deformation. In other words, the yield deformation is independent of the tab insertion angle and notch size. This is further confirmed in Fig. 17a, which shows that the specimens have similar yield deformation values. A similar conclusion can be drawn for $D_{F\text{-}Max}$ (Fig. 17b).

According to Fig. 17a, T4 to T6 have similar yield deformations. The reason is that the notch size and tab insertion angle have a counterbalancing effect on the yield deformation of this specimen group. Recall that the EN 12512 standard [25] was used to determine the yield point and the pre-peak force–deformation response was idealized into two linear parts. In the next two paragraphs, it will be shown that the first (initial) slope is affected by the notch size, and the second is influenced by the tab insertion angle. To further elaborate:

- The notches reduce the cross section area, and consequently, the joint stiffness decreases. As such, for any force value, the associated joint deformation would increase. Therefore, within the range of 10%–40% F_{max}, the deformation of the T4 specimens, which had the greatest notch size, was higher than that of the T5 and T6 specimens (Fig. 18). Since the initial slope includes the range of 10%–40% F_{max}, it is concluded that the notch size affects the initial slope.
- It is observed that the tab insertion angle affects $D_{F\text{-}Max}$. To further elaborate, recall that the cross section of T4 is reduced more than that of the T5 and T6 specimens (see Section 5.2.1).

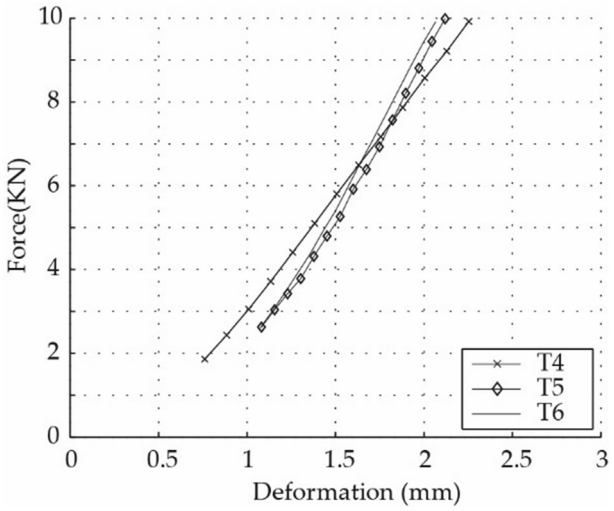

Fig. 18. Joint behavior between 0.1 and 0.4 * $F_{max.}$

Therefore, these specimens are weaker and experience earlier yielding at a lower force when compared to the symmetric specimens. During the experiments, it was observed that this earlier yielding prevents the T4 specimens from sudden damage. The reason is attributed to the earlier yielding, which enables the 45° angled specimens to undergo gradual damage and energy release; whereas, the symmetric specimens yield at higher forces and therefore release a greater amount of potential energy. Accordingly, the post-yield energy is gradually released in the asymmetric specimens. As such, at the maximum strength, the T4 specimens should undergo higher deformation when compared to the symmetric specimens. This explains why the T4 specimens have a greater $D_{F\text{-}Max}$ than the T5 and T6 specimens (Fig. 17b).

Thus far, it has been demonstrated that the effect of notch size counterbalances the effect of tab insertion angle for T4 to T6. In other words, although T4 has a lower initial stiffness, it has a larger $D_{F\text{-}Max}$. On the other hand, T5 and T6 have higher initial stiffnesses and smaller $D_{F\text{-}Max}$. Given that the yield deformation is a function of the initial stiffness and $D_{F\text{-}Max}$, it remains almost unchanged among the T4 to T6 (Fig. 17a) specimens. Fig. 19 shows the pair of idealized slopes for each specimen.

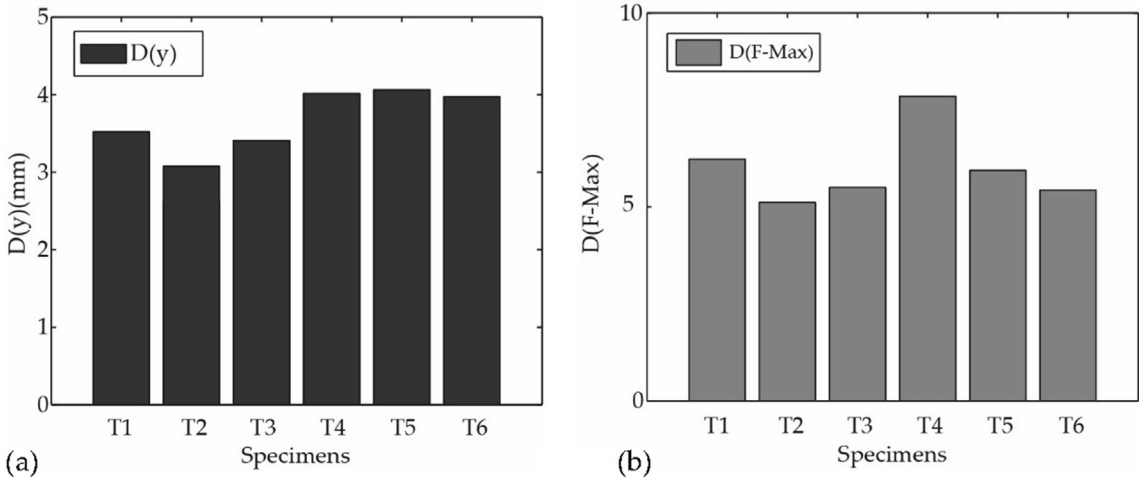

Fig. 17. Deformation at (a) yield and (b) peak strength ($D_{F\text{-}Max}$).

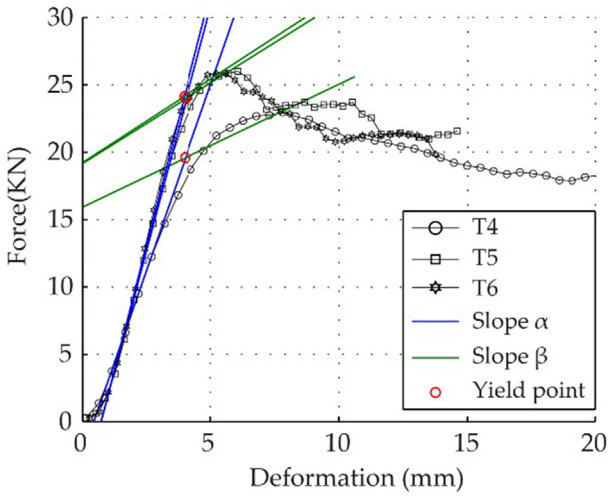

Fig. 19. Bilinear curve used to determine the yield point.

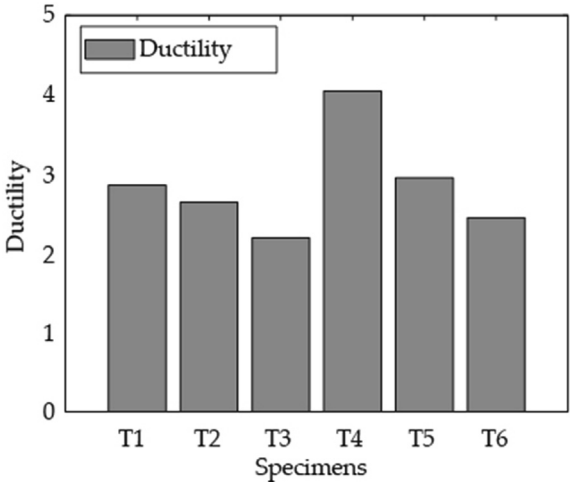

Fig. 21. Ductility of the TT joints.

5.2.3. Ultimate deformation

In Sections 5.1 and 5.2, the out-of-plane response of the joints was determined to be most influenced by the tab (tenon) insertion angle, the fiber orientation, and the notch size. The role of these parameters is even more pronounced in the post-peak behavior. As noted earlier, because the cross section is more reduced in the asymmetric joints (i.e. T1 and T4), these specimens experienced earlier yielding at a lower force than the others. Therefore, the damage propagates and the associated post-yield energy is released at a slower rate when compared to the other specimens. As such, the post-yield load-deformation behavior of these joints (T1 and T4) was smoother when compared to the other specimens (compare the load-deformation curves in Fig. 14b-c). Additionally, T1 and T4 had the highest D_u among all specimens, which decreased when the tab insertion angle changed from 45° to 60° (T2, and T5) and 90° (T3 and T6) (Fig. 20).

5.2.4. Ductility

The ductility demand, which is defined as the ratio between the ultimate (D_u) and yield deformation (D_y) (Eq. (3)), is used to quantify the ability of the joints to withstand deformations in the plastic range. Since the yield deformation is approximately the same across the fiber-parallel and fiber-perpendicular specimens (see 5.2.2 and Fig. 17a), the ultimate deformation governs the ductility of the specimens (see Eq. (3)). In general, the ductility decreased when the tab insertion angle increased from 45° to 90° (Fig. 21). This is primarily because the specimens with a 45° insertion angle had much higher post-yield deformations (see Fig. 20). Therefore, among all specimens, T1 and T4 had the highest ductility. More importantly, according to the Eurocode 8 [33], all of the tested TT joints are classified as having low ductility since $\mu \leqslant 4.0$. Additionally, the tensile, compressive, torsional, shear, and inter-fiber layer resistance contributes to the behavior of the TT joints, especially in the post-peak-force response phase. Since timber undergoes brittle response under direct tension, shear, and flexure (see [31,34] for more information), the TT joints generally demonstrate a non-ductile behavior. It is worth noting that the fiber-perpendicular specimens (T1 to T3) had a rapid propagation of damage beyond their peak strength, which directly affected the variability in the post-peak response. By examining the Coefficient of Variation (COV) for the associated parameters in Table 3, it is clear that the dispersion in μ is fairly significant ($COV_{average}$ = 0.22)

$$\mu = \frac{D_u}{D_y} \tag{3}$$

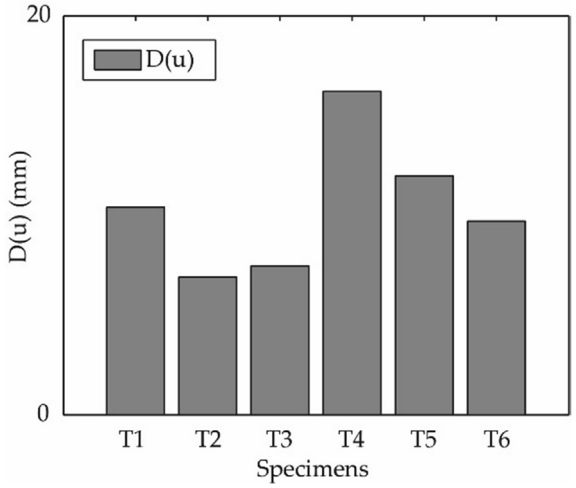

Fig. 20. Deformations at the ultimate strength.

6. Conclusions

An experimental investigation of the out-of-plane (flatwise) response of through-tenon (TT) joints was conducted. The performance of the joints was evaluated considering the effect of tab insertion angle and fiber orientation. Three tab insertion angles, 45°, 60°, and 90° and two fiber orientations, parallel and perpendicular to the loading direction, were considered.

Based on the low Coefficient of Variation (COV) observed in the pre-peak design parameters (i.e. stiffness, SLS/ULS strength and associated deformation), replicate-to-replicate variability was found to be minimal for each specimen. From the observed post-peak behavior, it was concluded that all of the tested specimens can be categorized as having low ductility. However, the strength degradation in the fiber-perpendicular specimens was faster compared to the fiber-parallel specimens. Additionally, it was determined that the initial load-deformation response is affected by the notch size, where joints with higher inclinations have greater notch sizes; and consequently, softer behavior.

For the fiber-perpendicular specimens, where the cross section consisted of 11 cross layers, very brittle failure was observed. The

failure was caused by the loss of the inter-fiber layer resistance. The yield and maximum strengths and the slip modulus remained almost unchanged among these specimens. For the fiber-parallel specimens, where the cross section included 11 longitudinal layers, the load-deformation behavior was deemed to be governed by the tab insertion angle, and the notch size. Better performance was observed compared to the fiber-perpendicular specimens and the following resisting mechanisms contributed to the load-carrying capacity: inter-fiber layer resistance, tension–compression, flexure, shear and torsional resistance of the fibers, and the embedment compression resistance. For both fiber-parallel and fiber-perpendicular specimens, the yield and maximum strength, as well as the stiffness of the 45°-angled specimens were small compared to the other specimens. This is because of the notch size of these specimens were greater than the others. Future studies should examine the role of notch size on the performance of the TT joints. This can be achieved by upscaling the dimension of the joints to decrease the role of the fabrication tools. In general, the ductility decreased when the tab insertion angle changed from 45° to 90°. Finally, the joints are classified as having low ductility.

CRediT authorship contribution statement

Aryan Rezaei Rad: Conceptualization, Investigation, Methodology, Software, Formal analysis, Data curation, Resources, Writing - original draft, Writing - review & editing, Visualization. **Henry Burton:** Conceptualization, Investigation, Methodology, Writing - original draft, Writing - review & editing, Supervision. **Yves Weinand:** Conceptualization, Supervision, Investigation, Writing - review & editing, Project administration, Funding acquisition.

Declaration of Competing Interest

The authors declare that they have no known competing financial interests or personal relationships that could have appeared to influence the work reported in this paper.

Acknowledgements

The support of the National Centre of Competence in Research (NCCR) Digital Fabrication (http://www.dfab.ch/) funded by the Swiss National Science Foundation (SNSF) is acknowledged (NCCR Digital Fabrication Agreement ID #51NF40141853). The support of École Polytechnique Fédérale de Lausanne (EPFL) is also acknowledged with many thanks.

Appendix A. Supplementary data

Supplementary data to this article can be found online at https://doi.org/10.1016/j.conbuildmat.2020.120001.

References

[1] R.W. Messler, Integral Mechanical Attachment: A Resurgence of the Oldest Method of Joining, first ed., Butterworth-Heinemann, 2006. doi: 10.1016/B978-0-7506-7965-7.X5018-4.
[2] A. Rezaei Rad, H. Burton, Y. Weinand, Performance assessment of through-tenon timber joints under tension loads, Constr. Build. Mater. 207 (2019) 706–721, https://doi.org/10.1016/J.CONBUILDMAT.2019.02.112.
[3] A. Rezaei Rad, Y. Weinand, H. Burton, Experimental push-out investigation on the in-plane force-deformation behavior of integrally-attached timber Through-Tenon joints, Constr. Build. Mater. 215 (2019) 925–940, https://doi.org/10.1016/J.CONBUILDMAT.2019.04.156.
[4] H.J. Blaß, J. Streib, Ingenious hardwood: BauBuche Beech laminated veneer lumber Design assistance for drafting and calculation in accordance with Eurocode 5, Pollmeier Massivholz GmbH & Co.KG, Creuzburg, Germany, 2017. https://doi.org/https://www.pollmeier.com/en/downloads/design-manual.html#gref.
[5] S. Roche, G. Mattoni, Y. Weinand, Rotational stiffness at ridges of timber folded-plate structures, Int. J. Sp. Struct. 30 (2015) 153–167, https://doi.org/10.1260/0266-3511.30.2.153.
[6] European Committee for Standardisation (CEN), CEN-EN 1995-1-1:2005+A1 - Eurocode 5: Design of timber structures - Part 1-1: General - Common rules and rules for buildings, Brussels, 2008.
[7] S.N. Roche, Semi-rigid moment-resisting behavior of multiple tab-and-slot joint for freeform timber plate structures, École Polytechnique Fédérale de Lausanne (EPFL) (2017).
[8] C. Schindler, Information-tool-technology: Contemporary digital fabrication as part of a continuous development of process technology as illustrated with the example of timber construction, in: Proc. Int. ACADIA Conf. 2007 Expand. Bodies, ACADIA, Halifax Nova Scotia, 2007.
[9] C. Robeller, M. Konaković, M. Dedijer, M. Pauly, Y. Weinand, Double-layered timber plate shell, Int. J. Sp. Struct. 32 (2017) 160–175, https://doi.org/10.1177/0266351117742853.
[10] R. Magna, M. Gabler, S. Reichert, T. Schwinn, F. Waimer, A. Menges, J. Knippers, From nature to fabrication: biomimetic design principles for the production of complex spatial structures, Int. J. Sp. Struct. 28 (2013) 27–39, https://doi.org/10.1260/0266-3511.28.1.27.
[11] J. Li, J. Knippers, Segmental timber plate shell for the landesgartenschau exhibition hall in schwäbisch gmünd—the application of finger joints in plate structures, Int. J. Sp. Struct. 30 (2015) 123–140, https://doi.org/10.1260/0266-3511.30.2.123.
[12] O.D. Krieg, T. Schwinn, A. Menges, J.-M. Li, J. Knippers, A. Schmitt, V. Schwieger, Biomimetic Lightweight Timber Plate Shells: Computational Integration of Robotic Fabrication, Architectural Geometry and Structural Design, in: Adv. Archit. Geom. 2014, Springer International Publishing, 2015, pp. 109–125. Doi:10.1007/978-3-319-11418-7_8.
[13] A.C. Nguyen, Y. Weinand, Development of a spring model for the structural analysis of a double-layered timber plate structure with through-tenon joints, in: 2018 World Conf. Timber Eng. WCTE 2018, Seoul, 2018. Doi:20.500.11850/314629.
[14] C. Robeller, M. Konakovic, M. Dedijer, M. Pauly, A Double-layered Timber Plate Shell - Computational Methods for Assembly , Prefabrication and Structural Design, in: Adv. Archit. Geom. 2016, vdf Hochschulverlag AG, Zürich, Switzerland, 2016:, pp. 104–122. Doi:10.3218/3778-4.
[15] P. Vestartas, N. Rogeau, J. Gamerro, Y. Weinand, Modelling Workflow for Segmented Timber Shells Using Wood-Wood Connections, in: Impact Des. With All Senses, Springer International Publishing, 2020, pp. 596–607. Doi: 10.1007/978-3-030-29829-6_46.
[16] A.C. Nguyen, P. Vestartas, Y. Weinand, Design framework for the structural analysis of free-form timber plate structures using wood-wood connections, Autom. Constr. 107 (2019), https://doi.org/10.1016/J.AUTCON.2019.102948 102948.
[17] A. Rezaei Rad, H.V. Burton, Y. Weinand, Macroscopic model for spatial timber plate structures with integral mechanical attachments, J. Struct. Eng. (United States) (2020), https://doi.org/10.1061/(ASCE)ST.1943-541X.0002726. In press.
[18] A. Stitic, A. Nguyen, A. Rezaei Rad, Y. Weinand, Numerical Simulation of the Semi-Rigid Behaviour of Integrally Attached Timber Folded Surface Structures, Buildings. 9 (2019) 55. Doi: 10.3390/buildings9020055.
[19] S. Roche, C. Robeller, L. Humbert, Y. Weinand, On the semi-rigidity of dovetail joint for the joinery of LVL panels, Eur. J. Wood Wood Prod. 73 (2015) 667–675, https://doi.org/10.1007/s00107-015-0932-y.
[20] M. Dedijer, S. Roche, Y. Weinand, Shear resistance and failure modes of edgewise Multiple Tab-and-Slot Joint (MTSJ) connection with dovetail design for thin LVL spruce plywood Kerto-Q panels, in: WCTE 2016 - World Conf. Timber Eng., Vienna University of Technology, Vienna, Austria, 2016, pp. 1516–1523.
[21] C.W.M. Robeller, Integral Mechanical Attachment for Timber Folded Plate Structures, École Polytechnique Fédérale de Lausanne (EPFL) (2015), https://doi.org/10.5075/epfl-thesis-6564.
[22] Pollmeier, About BauBuche, (2019). https://www.pollmeier.com/en/products/baubuche/baubuche-about.html#gref.
[23] CEN (European Committee for Standardization), EN 26891: Timber structures - Joints made with mechanical fasteners - General principles for the determination of strength and deformation characteristics, Brussels, Belgium, 1991.
[24] A. Hassanieh, H.R. Valipour, M.A. Bradford, Experimental and analytical behaviour of steel-timber composite connections, Constr. Build. Mater. 118 (2016) 63–75, https://doi.org/10.1016/J.CONBUILDMAT.2016.05.052.
[25] CEN (European Committee for Standardization), EN 12512: Timber structures – test methods – cyclic testing of joints made with mechanical fasteners, 2001.
[26] G.C. Foliente, Issues in seismic performance testing and evaluation of timber structural systems, in: CSIRO. Build. Constr. Eng. Ed. Int. Wood Eng. Conf., New Orleans, USA, 1996, p. 8.
[27] E. Karacabeyli, A. Ceccotti, Nailed wood-frame shear walls for seismic loads: test results and design considerations, Struct. Eng. World Wide (1999) 1–9.
[28] M. Yasumura, N. Kawai, Estimating seismic performance of wood-framed structures, in: Proc. 5th World Conf. Timber Eng., 1998, pp. 564–571.
[29] J. Milch, J. Tippner, M. Brabec, V. Sebera, J. Kunecký, M. Kloiber, H. Hasníková, Mechanical performance of lap scarf joint fastened using wooden dowel subjected to tension loading, in: WCTE 2018 - World Conf. Timber Eng., World Conference on Timber Engineering (WCTE), 2018.

[30] J. Bodig, B.A. Jayne, Mechanics of Wood and Wood Composites, Krieger Pub Co, 1993.
[31] C. Sandhaas, J.W.G. Van De Kuilen, Material model for wood, Heron. 53 (2013) 179–200.
[32] M. Gharib, A. Hassanieh, H. Valipour, M.A. Bradford, Three-dimensional constitutive modelling of arbitrarily orientated timber based on continuum damage mechanics, Finite Elem. Anal. Des. 135 (2017) 79–90, https://doi.org/10.1016/J.FINEL.2017.07.008.
[33] European Committee for Standardisation (CEN), CEN-EN 1998-1:2004 - Eurocode 8: Design of Structures for Earthquake Resistance - Part 1: General Rules, Seismic Actions and Rules for Buildings, Brussels, Belgium, 2004.
[34] A. Hassanieh, H.R. Valipour, M.A. Bradford, C. Sandhaas, Modelling of steel-timber composite connections: validation of finite element model and parametric study, Eng. Struct. 138 (2017), https://doi.org/10.1016/j.engstruct.2017.02.016.
[36] A. Rezaei Rad, Mechanical characterization of integrally-attached timber plate structures: experimental studies and macro modeling technique, École Polytechnique Fédérale de Lausanne (EPFL) (2020), https://doi.org/10.5075/epfl-thesis-8111.